A Radiance Model for Predicting Radio Wave Propagation in Irregular Dense Urban Areas

Eugenia Montiel, Alberto S. Aguado, and François X. Sillion

***Abstract*—We present a deterministic model of radio wave propagation based on radiance transfers. Our model uses radiosity techniques to determine facet-to-facet specular reflections according to a three-dimensional building description. The model contains two main components. First, visibility between elements is determined and used to establish links that represent radiance transfers that include diffraction and free space losses based on geometric approximations. Second, links are used to define a transfer equation whose solution provides the transfer intereflections. The solution is obtained by using hierarchical techniques. The results of the model show good agreement with measurements made in urban areas.**

***Index Terms*—Pathloss prediction, propagation, radiance.**

I. Introduction

THE GROWTH of wireless communications and the introduction of cellular communications to support a high density of users in dense urban areas have motivated considerable interest in the simulation and prediction of radio wave propagation in urban environments. Path-loss can be computed by using empirical prediction models that include factors to account for the urbanization, topology and antenna features [1]–[3]. Although these models are valuable tools for estimating signal propagation, they generally produce significant errors for small covering ranges [4] (i.e., less than 1 km), for low base station antennas and for irregular dense coverage areas. A major source of error is due to buildings of different size and irregular passageways. In these cases, deterministic models can produce more accurate path loss predictions [4]–[11].

Deterministic models use detailed two-dimensional (2-D) or 3-D geometric descriptions of the urban area to compute radio wave propagation [12], [13]. A detailed description of the geometry makes it possible to obtain a detailed path-loss prediction by modeling the power being transferred from one point to another. There are two main approaches to model power transfers: ray tracing and energy transfers. In the ray tracing approach, dominant paths determine points at which to evaluate the intensity. Paths are computed by considering diffraction and reflection between elements such as building's facets and edges. Reflected and refracted rays are fired at each intersection from the path. This approach provides an accurate treatment of specular reflection and has been extensively exploited in radio wave propagation models. In a divergent approach, instead of firing rays from a point, it is possible to model transfers of energy by considering all the paths in which a signal can reach a point. Thus, the intensity at every point can be found by solving a system of equations that account for the reflection and absorption of all surfaces simultaneously. This approach is based on radiosity models derived from thermal-engineering concepts [14] and it has been extensively used in the simulation of light [15]. The main advantage of this approach is that it provides an accurate treatment of inter-object reflections. However, radiosity models have not been very popular in radio wave propagation [16]–[18]. The main drawback is that radiosity is expressed as a uniform dispersion, thus it does not model any specular component. As such, it requires complementary models to account for diffuse reflections [18], [19]. Additionally, radiosity models do not include diffraction and multipath fading. This paper develops a model that addresses these problems. Our model avoids the use of radiosity in favor of a development in terms of radiance that includes a model of the reflectance function. The reflectance function contains specular and diffuse components. Additionally, we model the interaction between facets by including diffraction and multipath fading.

II. Global Radiance Framework

Fig. 1 illustrates the main elements of our prediction model. The model uses a 3-D description containing the facets and the edges defining the buildings within a geographic area. The visibility between edges and facets is computed in two steps. In the first step, the 3-D space is subdivided into a set of elements forming a regular grid. In the second step this grid is used to determine the existence of line-of-sight between edges and facets. The grid and visibility information are stored in the city database. As a result, they can be reused for alternative transmitter locations.

In order to reduce computation, the prediction area is bounded based on the fourth-power distance [20]. This bounding criterion produces an excess loss, so areas with insignificant power contributions are excluded from the prediction. The bounded area and the precomputed visibility are used to select the edges and facets that have a direct line-of-sight to the transmitter or to the receiver. High-order reflections are included by considering elements visible from the selected elements.

Once the elements that will contribute significantly to propagation have been selected, propagation links are defined. A link

Manuscript received July 24, 2001; revised October 28, 2002. This work was supported by Alcatel Mobile Communications, France under Grant UPM 8-98

E. Montiel was with the Centre for Communications Systems Research (CCSR), University of Surrey, Guildford, GU2 7XH U.K. She is now with Cellular Design Services Ltd., Horsham, West Sussex, RH12 4QD U.K.

A. Aguado was with the Centre for Vision, Speech and Signal Processing, University of Surrey, Guilford, GU2 7XH U.K. He is now with Character Core Group, **[AUTHOR: PLEASE PROVIDE THE COMPLETE NAME OF THE COMPANY, CITY AND POSTAL CODE]** EA, U.K.

F. Sillion is with the INRIA, ARTIS/GRAVIR, 38330 Montbonnot, France.

Digital Object Identifier 10.1109/TAP.2003.818781

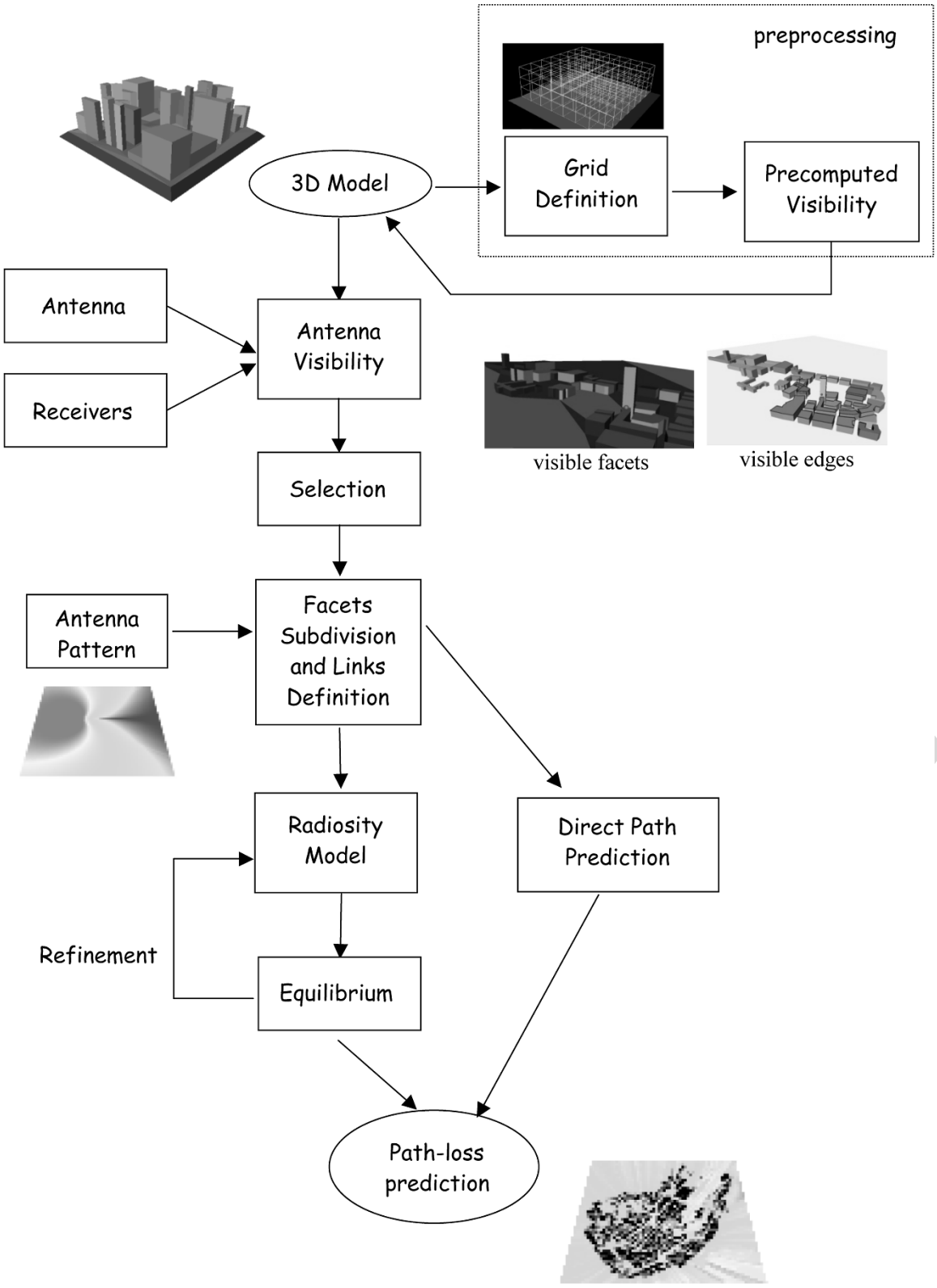

Fig. 1. Global radiosity framework.

indicates that the signal is propagated between facets by means of reflection or diffraction. A facet can have many incoming and outgoing links, forming a network in which each facet can be considered either as a multipath receiver or as a multipath transmitter. A radiance equation is used to model the propagation between the facets in a link. The model is defined as the vector sums of many paths resulting from reflection and diffraction. Since the direct path from the receiver to the transmitter does not have a reflection or diffraction component, the contribution for this path is not included in the radiance model. The transfer

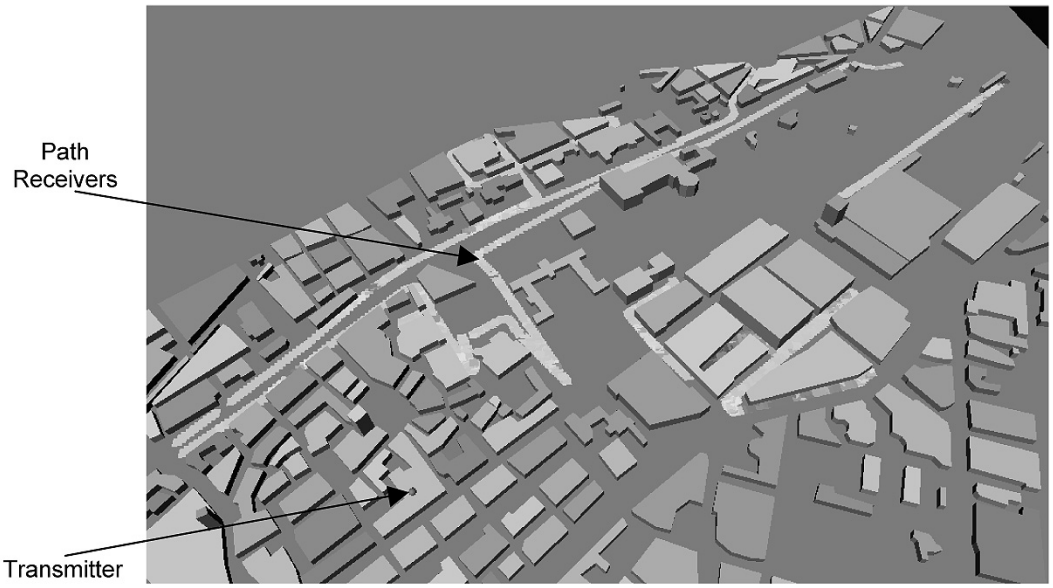

Fig. 2. City data with one antenna and a path of receivers.

of this link is computed separately and then included in the final path loss prediction (see Fig. 1).

The global transfer solution is obtained by using hierarchical techniques. These techniques compute all possible paths of energy transfers at variable levels of resolution [15], [21]. Facets are subdivided into small surfaces, forming a hierarchical data structure. Thus, the interaction between two surfaces is represented at different levels of detail. The subdivision models accurate transfers between finite small areas. This makes computations efficient and it accounts for partial occlusions. The transfer solution in a hierarchical model is then obtained by repetitively updating the energy transfers until the updates of the incident and emitted energies are small.

III. Database

Our database contains information about building geometry, antenna patterns and field measurements. The building database contains 303 buildings distributed over approximately an area of 1×1 km in the Stuttgart region. Fig. 2 shows a snapshot of the 3-D building database. The database provides geometric information. It does not contain any reflectance properties of the buildings.

We organized the building data following a hierarchical-geometric representation. A city is represented as a list of buildings. Each building is represented as a list of facets, each facet is composed of edges, each edge has two vertices, and a vertex is defined as a 3-D point with (x, y, z) coordinates. Facets are defined as closed polygons that represent the roof and walls. Buildings are approximated by considering only vertical walls and horizontal roofs.

The database contains the position of two rooftop transmitters whose patterns are defined as the gain for the far-field region as a function of directional coordinates. We have the absolute orientation of the antenna pattern for each transmitter. The antenna pattern is specified only at selected orientations in horizontal and vertical planes crossing at the emitter location. This data is interpolated to obtain the attenuation in any direction. Field measurements in the 800 MHz band are defined as a path of 2-D positions with a height of 1.7 m. Measurements were obtained from the two independent transmitters. Fig. 2 shows the position of one transmitter and the corresponding field measurements path.

IV. Visibility

In order to compute propagation, we need to determine which building facets reflect and receive direct reflection and diffraction from other buildings. Reflection is produced when two facets have a direct line-of-sight, whilst diffraction is produced when an edge has a direct line-of-sight with two facets.

We compute visibility in two stages. First, we compute the visibility between the geometric elements in the 3-D model. Since this visibility is independent of the location of the transmitter and the receivers, it is precomputed and stored within the database. In a second step, we determine which geometrical elements have a direct line-of-sight with the receivers and with the transmitter. The visibility between two elements is determined by considering the visibility between two points. For a facet, if one of its corners is visible, then we consider that the facet is visible. For an edge, if one of its two end-points is visible, then we consider that the edge is visible. Additionally, edges in the same facet are considered visible to each other. This visibility computation determines weather a facet or part of it contributes to the path loss. This information is then used by the hierarchical algorithm to divide the facets in such a way that the visibility, the point of reflection and the actual area contributions (due to partial occlusions) are accurate. Thus, transfers occur between small areas of visible facets (Section V-F).

In order to determine visibility, we need to look for an intersection between the planes that define facets and the straight line that joins a pair of points. Given the large number of facets in a typical urban area, the computation of the visibility for all the

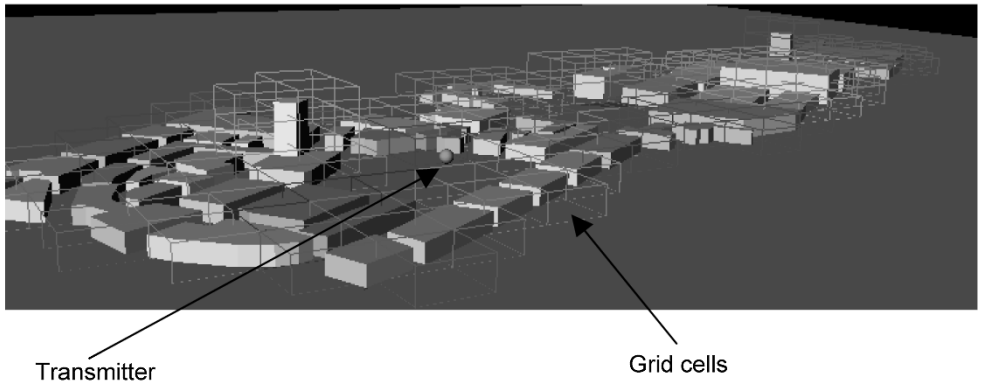

Fig. 3. Example of 3-D partition used during visibility computations.

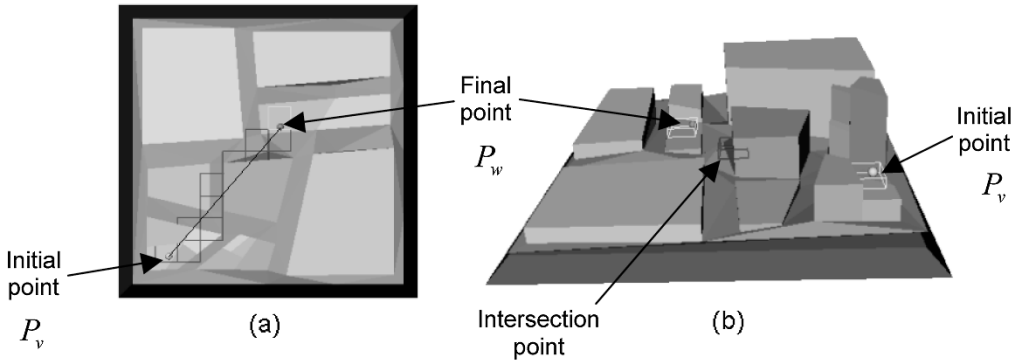

Fig. 4. Example of grid elements selected during the computation of the visibility between two points. (a) Top view of the grid trajectory. (b) 3-D grid element for the initial, final and intersection points.

elements in the model requires significant computational load. This is a demanding task even if visibility in the 3-D model is precomputed. In order to reduce this complexity, we use a space volumetric partitioning technique. This technique is related to partitioning visibility algorithms [22], [23], but instead of computing a graph that specifies what can be seen from a given point, we use the subdivision to search for intersections. That is, we reduce the number of intersection tests by reducing the number of facets to a predetermined region near to the tested line.

Fig. 3 shows an example of the partition of the 3-D space for a subset of buildings in the database. The partition divides the space into a set of cubes that define a 3-D grid. The size of the grid is given by the average of the size of the buildings; thus, we expect to have about one building per cube. Each cube contains a list to store the buildings that are intersected by its volume. Since the grid is independent of the location of the transmitter and the receivers, it is precomputed and stored in the city database. The elements of the grid reduce computations by limiting the intersection tests to facets contained in the elements that define the trajectory of the straight line between two points. Fig. 4 shows an example of the use of grid elements in the computation of visibility. Fig. 4(a) shows a top view with the elements that define the trajectory between two points. Fig. 4(b) shows a 3-D view of the initial, final and the intersection points obtained by the algorithm. Given two points p_v and p_w, grid elements are incrementally computed by considering the trajectory of the line-of-sight given by

$$\Gamma_{v,w} = p_v + q_{v,w}t \tag{1}$$

where $q_{v,w} = (p_w - p_v)/||p_w - p_v||$ is the normalized vector defining the direction of the line. The trajectory of the line defines a list of consecutive elements of the 3-D grid. The first element in the list is the element of the grid that contains the point p_v. The last element in the list is the grid element that contains the point p_w. Given a grid element e_k, the next grid element e_{k+1} in the list can be obtained by determining the intersection of the line in (1) with the six planes that form the cube of the element e_k. The element e_{k+1} must be chosen in the direction of the plane that is first intersected by the line. This process is illustrated in Fig. 5. In this figure, we indicate in grey the planes that are intersected by the line $\Gamma_{v,w}$. The planes Ω_1 and Ω_2 are intersected one after the other. As such, the element e_{k+1} is the grid element that shares the facet Ω_2 with the current element e_k.

We represent planes by considering the homogeneous form

$$\Omega^T p = 0 \tag{2}$$

where $\Omega^T = [A \;\; B \;\; C \;\; D]$ and $p^T = [x \;\; y \;\; z \;\; 1]$. Thus, the intersection with the line $\Gamma_{v,w}$ is given by

$$t = \frac{\Omega^T p}{\Omega'^T q_{v,w}} \tag{3}$$

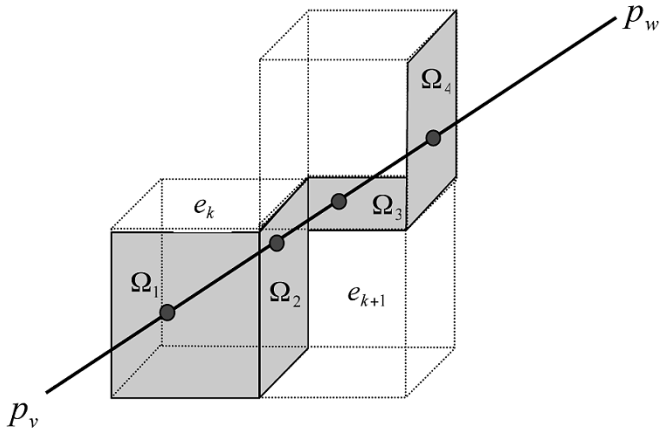

Fig. 5. Example of consecutive grid elements.

where $\Omega'^T = [A\ B\ C]$ are the reduced coordinates of the plane.

In order to determine the visibility, we look for an intersection with the building's facets in each new grid element in the trajectory. This is performed by evaluating (3) for the planes defined by the facets of the buildings stored in the current grid element. If an intersection with a facet is found, then the points are not mutually visible and the search for the grid elements defining the line trajectory is stopped. If the facets of the building in the grid element do not produce an intersection, then we verify for other grid elements in the trajectory until the grid element containing the point p_w is reached. If we reach the last element in the trajectory, then we consider that the points are visible. The example in Fig. 4(b) shows the case when an intersection is found in the trajectory. Fig. 6 shows two examples of the results obtained with the visibility computation process. In this figure, we highlight the facets and edges that are visible from a transmitter position. Fig. 6(a) shows the visible facets and Fig. 6(b) shows the visible edges.

V. Radiance Model

A. Radiance and Radiosity

In a deterministic model, predictions are obtained by modeling energy transfers. However, energy can be represented by alternative physical quantities such as power, irradiance, radiant exposition, radiosity or radiance. These radiometric definitions can be used to express the energy emitted or travelling through space and they can be related to reflection, diffraction, incidence and emittance phenomena. The effective radiated power (ERP) is defined as the product of the radiated power P and a dimensionless gain $G(\theta, \varphi)$. That is, $PG(\theta, \varphi)$. This measure can be used to obtain the power at a terminal at a distance d by including a factor that accounts for free space propagation. For example, power flow at a distance d for an isotropic transmitter in free space is given by $PG(\theta, \varphi)/4\pi d^2$. The term $PG(\theta, \varphi)/4\pi$ defines the radiant intensity [24] and it measures the power leaving an area in a particular direction. This measure is very useful for modeling the received and the transmitted power between point resources. However, to model the incident and the reflected power between surfaces, it is necessary to account for surface orientation and area. This can be achieved by considering the radiance of a surface [24].

If a surface radiates power into a hemisphere, its radiant intensity is given by

$$I(\theta, \varphi) = \frac{PG(\theta, \varphi)}{2\pi}. \tag{4}$$

The radiance of a surface is the power per unit of foreshortened area of the source (projected area) per solid angle. If a surface has an area A, then the radiance is $L(\theta, \varphi) = (PG(\theta, \varphi)/2\pi)/A\cos(\theta)$. That is

$$L(\theta, \varphi) = \frac{I(\theta, \varphi)}{A\cos(\theta)}. \tag{5}$$

Fig. 7 illustrates the concept of radiant intensity and radiance for a 2-D slice of the hemisphere. The term $A\cos(\theta)$ defines an approximate value of the projection of A into the hemisphere. This is only an approximation since the projected area is computed as a tangent plane. Thus, accurate modeling requires small areas.

Radiosity defines the radiant power emitted into the hemisphere per unit area. That is

$$B = \int_{\Omega} I(\theta, \varphi) d\omega. \tag{6}$$

This measure is independent of direction. For diffuse surfaces, radiance is defined as $L = L(\theta, \varphi)$. Thus, $B = L\pi$. The radiosity equation [25] uses this uniform dispersion property to express the radiosity of a set of surfaces as the sum of the emitted and reflected radiosity of the other surfaces [14], [15], [26]. As such, the power in each surface can be obtained by solving a system of equations whose solution represents the energy equilibrium. That is, a point where the reflected power is equal to the incident power plus the constant emittance. In this paper, we consider the energy in terms of radiance. Radiance maintains the directional dependence and it can include specular and diffuse components by modeling reflections by a reflectance function. Additionally, it can be used to model diffractions and fading due to multiple path propagation. Our model can be described by two main components: (i) geometric relationships and (ii) energy transfers. The first component is defined by transfer links and the second component by means of an equilibrium equation.

B. Transfer Links

The propagation between facets is performed by defining links that model the transfer of energy from one surface to the other. An accurate model requires consideration of small facets for which the geometry of the transfer (energy transfer and occlusion) can be correctly approximated. As such, for each pair of visible surfaces, we create a set of links by using a subdivision process that stops when the error in the geometric approximation (the unoccluded form factor in (17)) is smaller than a fixed threshold. The recursion maintains a hierarchy of subfacets representing different levels. Links are established only if surfaces are visible according to the following two cases.

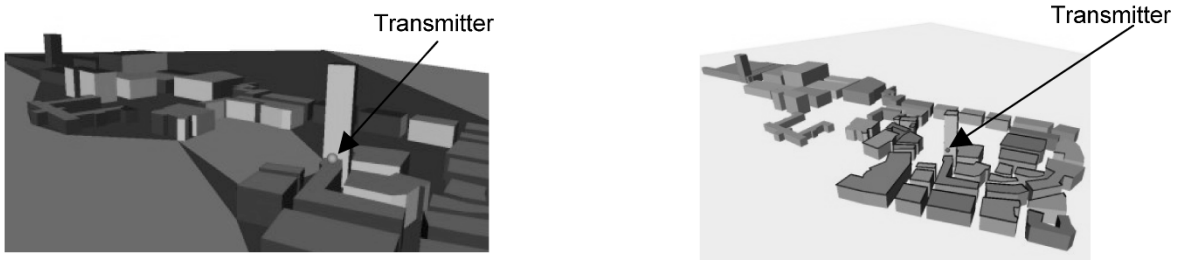

(a) (b)

Fig. 6. Visibility results. (a) Example of visible facets. (b) Example of visible edges.

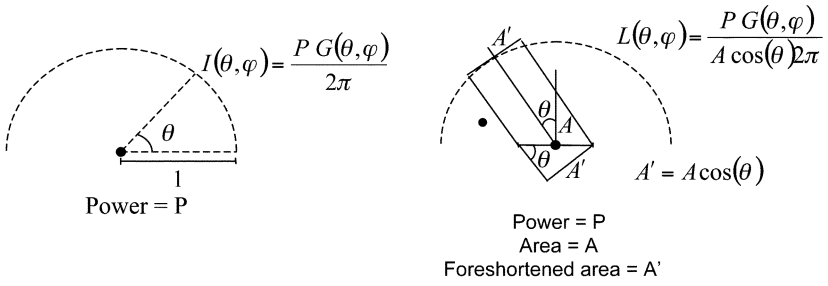

(a) (b)

Fig. 7. Radiant intensity and radiance of a surface. (a) Radiant intensity measures the power leaving a point per solid angle. (b) Radiance measures the power per unit of foreshortened area per solid angle.

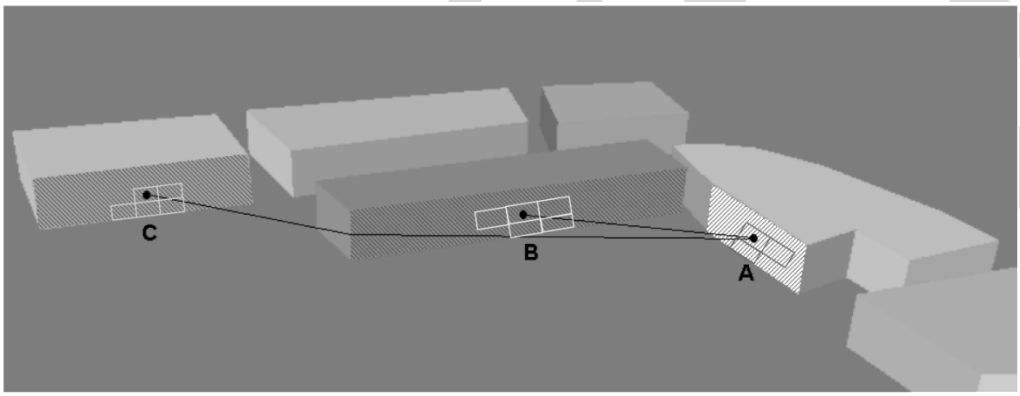

Fig. 8. Example of transfer links. The link between A and B models reflection and the link between A and C models a single diffraction.

First, when there is a direct line-of-sight between the facets. Secondly, when two facets do not have direct line-of-sight, but they have a direct line-of-sight to a common edge. This last case includes multiple diffractions. That is, when there is a succession of edges that maintain a direct line-of-sight. Fig. 8 illustrates two examples of links with reflection and diffraction effects. The link between the small patches A and B models reflection. The link between patches A and C models a single diffraction.

The link from the facet v to the facet w is denoted as $H_{v,w}$. $H_{v,w}$ represents a dimensionless factor defining the fractional amount of power radiated from the facet w that is radiated by the facet v. The radiance transfer equation [27], [28] models the outgoing radiance of the facet v as the sum of the incident radiance from the other surfaces. That is

$$L_v(\theta_o,\varphi_o) = \sum_w H_{v,w} L_w(\theta,\varphi) \tag{7}$$

where $L_w(\theta,\varphi)$ denotes the radiance of the w^{th} facet in the direction (θ,φ) and $L_v(\theta_o,\varphi_o)$ denotes the radiance reflected by the v^{th} facet. Equation (7) provides a model of the power transported between surfaces. Variables may be either radiance intensity [29] or radiant power [30]. We use this equation to provide a simplified model of the power transported between two surfaces. In our model, the factor $H_{v,w}$ is defined by

$$H_{v,w} = D_{v,w} G_{v,w} F_{v,w}. \tag{8}$$

The components in this equation model the diffraction $(D_{v,w})$, the power transfer $(G_{v,w})$ and the fading phasor $(F_{v,w})$.

In (8), $D_{v,w}$ represents the multiplicative loss due to diffraction. In general, diffraction losses can be computed by considering any multiple edge diffraction method. In the results presented in this paper, the loss is determined based on the Deygout method [1]. This method is computationally simple and it pro-

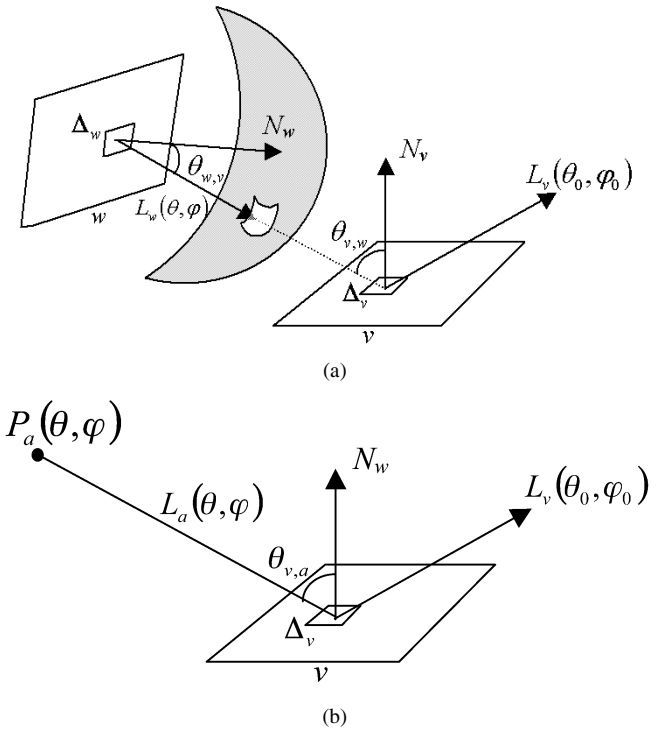

Fig. 9. Geometry of radiance transport. (a) For two facets. (b) For the antenna and a facet.

vides accurate results for a small number of edges. The diffraction parameter

$$V_{v,w} = 2\sqrt{\frac{((d_{v,k} + d_{k,w}) - d_{v,w})}{\lambda}} \tag{9}$$

is used to determine the loss. In this equation, d denotes the distance between the facets v and w and the edge k.

The factor $G_{v,w}$ in (8) represents the direct path loss and it includes attenuation due to reflectivity and geometry. In order to determine this factor, we consider pair-wise exchanges between the facets, the transmitter and the receiver. This factor is explained in Sections V-C and V-D. The phase fading factor $F_{v,w}$ is explained in Section V-E.

C. Direct Path Loss Between Two Facets

Fig. 9(a) illustrates the geometry between two facets. We are interested in obtaining the outgoing radiance $L_v(\theta_o, \varphi_o)$. First, we determine the incident power in the v^{th} facet. Since radiance is given in unit of projected area, then the radiated intensity in (5) for an infinitesimal area Δ_w is given by

$$I_w(\theta,\varphi) = L_w(\theta,\varphi)\cos(\theta_{w,v})\Delta_w \tag{10}$$

where $\theta_{w,v}$ is the angle between the surface's normal and the straight line between the surfaces. The value of $I_w(\theta,\varphi)$ is the power delivered toward the v^{th} facet. Only a fraction of this power reaches the v^{th} facet. This fraction is determined by the projection of the infinitesimal area Δ_v into the hemisphere of the surface w. That is,

$$\Phi = \frac{\cos(\theta_{v,w})\Delta_v}{d_{v,w}^2} \tag{11}$$

Thus, by using (5) the incident power is [15]

$$I_v(\theta,\varphi) = L_w(\theta,\varphi)\frac{\cos(\theta_{w,v})\cos(\theta_{v,w})}{d_{v,w}^2}\Delta_v\Delta_w. \tag{12}$$

The power reflected by the surface depends on its reflectance properties. We denote the bidirectional reflectance of the surface as $\rho_v(\theta,\varphi,\theta_o,\varphi_o)$. This is expressed in inverse steradian units (sr^{-1}). Note that for Lambertian reflectors the reflectance is independent of the incidence and reflectance directions. Thus, in radiosity models the reflectance is given as the ratio of reflected power to incident power defined as the one-dimensional reflectance constant $\pi\rho_i$ [31]. In our model, we consider the more general definition

$$\rho_v(\theta,\varphi,\theta_o,\varphi_o) = \frac{L_v(\theta_o,\varphi_o)}{E_v(\theta,\varphi)} \tag{13}$$

where the irradiance $E_v(\theta,\varphi) = I_v(\theta,\varphi)/A_v$ defines the incident power per unit of area and A_v represents the area of the v^{th} facet. Thus, (12) can be rewritten to express the relationship between the radiance of the facets as

$$L_v(\theta,\varphi) = L_w(\theta,\varphi)\rho_v(\theta,\varphi,\theta_o,\varphi_o)\frac{\cos(\theta_{w,v})\cos(\theta_{v,w})}{A_v d_{v,w}^2}\Delta_v\Delta_w. \tag{14}$$

The bidirectional reflectance function models the directional dependence of the transmission. We model reflection by the isotropic component in the Phong model [32]. That is

$$\rho_v(\theta,\varphi,\theta_o,\varphi_o) = c_v\cos^n(\alpha) \tag{15}$$

where α is the angle between the perfect mirror outgoing vector and the outgoing vector. The parameter c_v models absorption and the specular-reflection exponent n controls the aperture of the reflection. High values of n model sharp focused reflections and $n = 0$ for perfect diffuse surfaces. Thus, the bidirectional response in (14) is

$$F_{v,w}(\theta,\varphi) = c_v\frac{\cos^n(\alpha_{v,w})\cos(\theta_{w,v})\cos(\theta_{v,w})}{A_v d_{v,w}^2}\Delta_v\Delta_w. \tag{16}$$

For finite areas, we consider that the energy incident on the surface of the v^{th} facet is the sum of the energy at each point. However, each point receives power for each point in the w^{th} facet. Thus, since radiance is measured by unit of area, we have that

$$F_{v,w}(\theta,\varphi) = \int_{\Delta_v}\int_{\Delta_w} c_v\frac{\cos^n(\alpha_{v,w})\cos(\theta_{w,v})\cos(\theta_{v,w})}{{A_v}^2 d_{v,w}^2}d_v d_w. \tag{17}$$

D. Path Loss for an Antenna and a Facet

In the previous section, we considered the emitted radiance of a facet due to the radiance of another facet. In this section we shall consider the relationship between the radiance of a facet and the receiver and transmitter power. In radiosity techniques, it is possible to multiply radiosity by area, so the transfer equation can be expressed in terms of total power emitted into the

hemisphere [18], [33]. However, power is expressed as a uniform dispersion. In order to keep power dependent on the ingoing and outgoing directions we consider two propagation phenomena. First, we use the concept of radiance intensity to determine the power incident on the facet. Secondly, we use the reflectance and the geometry of the facet to obtain the emitted radiance by following the plane surface model [20]. Fig. 9(b) illustrates the geometry between a transmitter and a facet. We are interested in obtaining the outgoing radiance $L_v(\theta_o, \varphi_o)$ given the transmitter power $P_a(\theta, \varphi)$. Here the subindex a is used to denote measurement for the point source a.

The radiant intensity of a transmitter with a radiant power P_a and gain $G_a(\theta, \varphi)$ is given by

$$I_a(\theta, \varphi) = \frac{P_a G_a(\theta, \varphi)}{4\pi}. \tag{18}$$

This defines the power in the direction (θ, φ) per steradian. The free-space equation

$$I_a(\theta, \varphi) = \frac{P_a G_a(\theta, \varphi) G_r \lambda^2}{4\pi d^2} \tag{19}$$

can be obtained by considering a receiver at distance d with an effective area $A_a \approx \lambda^2/4\pi$ and gain G_r. However, we do not have a point-receiver at the other end, but we are interested in obtaining the power incident on a small flat area. Thus, we need to consider the distance, the area and the surface orientation. The angular aperture of a surface at a distance $d_{v,a}$ with a small area Δ_v and with an angle $\theta_{v,a}$ [Fig. 9(b)] is given by

$$\Phi = \frac{\cos(\theta_{v,a})}{d_{v,a}^2} \Delta_v. \tag{20}$$

Thus the incident power is

$$I_v(\theta, \varphi) = P_a G_a(\theta, \varphi) \frac{\cos(\theta_{v,a})}{4\pi d_{v,a}^2} \Delta_v. \tag{21}$$

Once we know the incident power, we can obtain the emitted radiance by considering the reflected angle geometry of the facet. By considering (13) we have that the radiance of the facet is

$$L_v(\theta, \varphi) = P_a G_a(\theta, \varphi) \rho_v(\theta, \varphi, \theta_o, \varphi_o) \frac{\cos(\theta_{v,a})}{4\pi d_{v,a}^2} \Delta_v. \tag{22}$$

If the bidirectional reflectance function is given by (15), then we have

$$F_{v,a}(\theta, \varphi) = c_v \frac{\cos^n(\alpha_{v,a}) \cos(\theta_{v,a})}{4\pi d_{v,a}^2} \Delta_v. \tag{23}$$

For a finite area, we must consider that the energy incident on the surface of the v^{th} facet is the sum of the energy at each point. Thus

$$F_{v,a}(\theta, \varphi) = \int_{\Delta_v} c_v \frac{\cos^n(\alpha_{v,a}) \cos(\theta_{v,a})}{4\pi A_v d_{v,w}^2} d_v. \tag{24}$$

To model the power at a point-receiver, we compute the incident power from a facet and then we multiply it by the effective area of the receiver. The radiated intensity of a facet for an infinite area is given in (10). The available power for a receiver at a distance $d_{v,r}$ is

$$I_r(\theta, \varphi) = G_r L_v(\theta, \varphi) \frac{\lambda^2 \cos(\theta_{v,r})}{4\pi d_{v,r}^2} \Delta_v. \tag{25}$$

Here, the factor $\lambda^2/4\pi d_{v,r}^2$ defines the effective area, and G_r is the gain of the receiver antenna. For a finite facet area we have

$$I_r(\theta, \varphi) = \frac{\lambda^2 G_r}{4\pi} \int_{A_w} L_w(\theta, \varphi) \frac{\cos(\theta_{w,v})}{d_{v,w}^2} d_w. \tag{26}$$

E. Phase Shift

In order to include channel fading, propagation (Section V-A) should include in-phase and quadrature-phase components. These components are determined based on the dominant component incident on each facet. That is, if the angle of the dominant phasor of a facet w is γ_w, the arriving wave at facet v experiences a phase shift of

$$\gamma_w + \alpha_{w,v} \tag{27}$$

where $\alpha_{w,v}$ is the shift in a distance $d_{v,w}$. Thus, in order to compute the fading interference, we define the last factor in (8) as

$$G_{v,w} = e^{i(\gamma_w + \alpha_{w,v})}. \tag{28}$$

Thus, (7), actually defines a vector sum. In practice, we use the modulus

$$L_v(\theta_o, \varphi_o) = \left\| \sum_w H_{v,w} L_w(\theta, \varphi) \right\| \tag{29}$$

to obtain the transfer power and we consider γ_v to be the phase shift for the incident link with the strongest power.

F. Transfer Equation

Equation (29) models the energy transfer from a surface to another. The unknowns of this equation are the radiances L_v and L_w. Similarly to the radiosity equation [25] this equation defines a system where each row v determines the radiance as the weighted sum of the radiance of other surfaces. However, it represents the reflected energy as a function rather than as single value. Reflected energy functions have been studied in [31] and [34]. In our implementation, the solution is obtained by considering discrete values of the functions $L_v(\theta_o, \varphi_o)$ and $L_w(\theta_o, \varphi_o)$. The discrete values L_{w,θ_o,φ_o} define the radiance in a particular direction. Thus

$$L_{v,\theta_o,\varphi_o} = \left\| \sum_w H_{v,w} L_{w,\theta,\varphi} \right\|. \tag{30}$$

In order to find the solution, we first use (22) to compute the radiances for facets that have a link to the transmitter. This gives an initial emittance value to some facets. This initial value is transferred to other facets in an iterative process. In each step, the radiance of each facet is updated by gathering the incoming power from other surfaces. The update process is repeated until

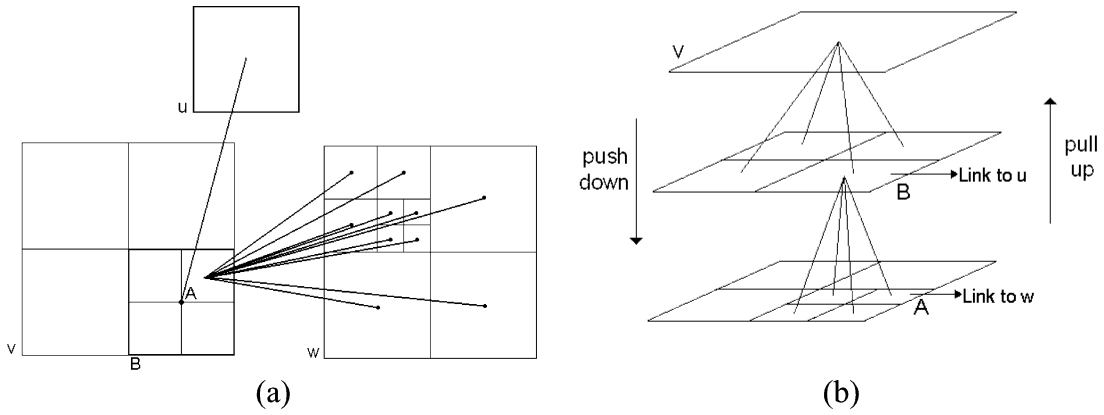

Fig. 10. Power transfer between two surfaces. (a) Subdivision and links. (b) Hierarchical representation of the patches in facet v.

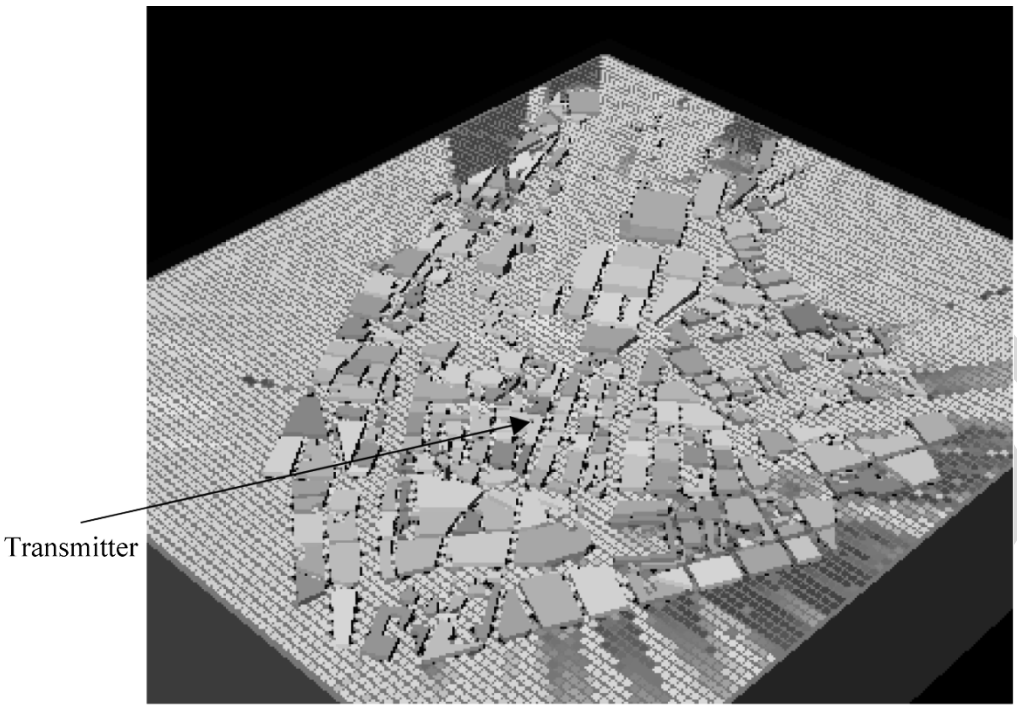

Fig. 11. Result of path-loss prediction.

the transfer from surfaces is insignificant. Our implementation updates incoming power by using hierarchical gathering [15], [21]. In this approach, facets are subdivided into small patches, so visibility and power can be accurately computed.

Fig. 10(a) illustrates the gathering process from two facets. Facets are subdivided into patches that are stored in a quad-tree structure. Each patch in the subdivision represents a new reflector that is linked to other facets. In the example, patch A has a link to each of the patches in the facet w. Patch B includes patch A and it has a link to surface u. These links are used to gather the power contribution to the surface v. Gathering is performed by following the links originated at each facet. Fig. 10(b) shows the hierarchical representation of surface v. Notice that links to other surfaces are defined at different levels in the hierarchy. Once the radiance for the patches in a surface has been gathered, it is necessary to integrate the radiance at all levels. This is achieved by a bidirectional traversal algorithm implemented in two steps. In the first step, accurate values at the lowest level (i.e., smallest subdivision) are obtained by adding the contributions of each subdivided facet. That is, starting from the top of the hierarchy, the power of the subelement is added to each of its descendants to push down correct power values. In the example in Fig. 10, this process will add to the radiance in patch A, the radiance computed at the coarse patch B. Thus, the new radiance in A contains all the contributions for all the facets at different levels of detail.

The second step in the traversal algorithm updates the values in the hierarchy by pulling up the values from the finest detail. This process computes the value of a larger patch by combining the value of its subpatches. This step ensures that iterations performed at any level in the hierarchy have accurate radiance. Since we are modeling power per unit of area, then the values of a patch are given by the weighted-area average of the values of its subpatches. In Fig. 10, the radiant value in patch B is computed by combining the radiant value of its subpatches. Since A

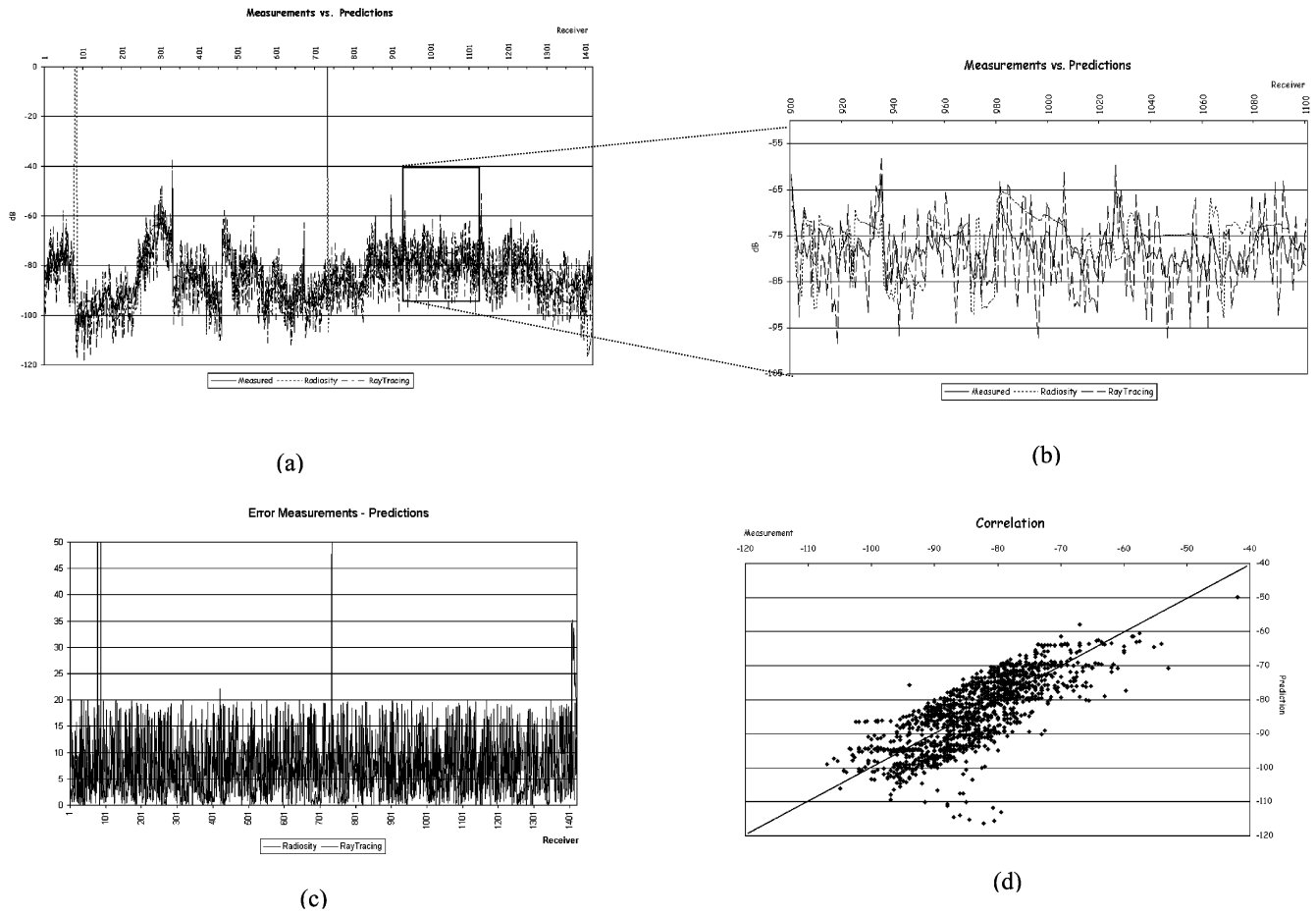

Fig. 12. Comparison of predicted values versus measurements for the transmitter located at Karstadt. (a) Measurements versus Predictions. (b) Detail of Measurements versus Predictions. (c) Error between measurements and predictions. (d) Correlation between Measurements and Predictions.

contains all the contributions for all the facets at different detail, then B will consistently include the contribution at all levels.

VI. Results

The model was used to predict path-loss for two transmitter positions. We use a single value of c_v and n, in (15), for all buildings ($c_v = 0.86$, $n = 18$). These values were obtained by minimizing the prediction error. Fig. 11 shows the prediction results obtained for the transmitter located at Karstadt. Since at the border of the city there are not buildings that reflect the signal back, then shadows are produced. However, we can see how the reflection and diffraction make accessible the signal in the corridors formed by buildings. The image shows a congruent prediction with the data base configuration. To validate the results, we compare the prediction against field measurements. The graphs in Figs. 12 and 13 show the measurements, predictions, error and correlation for the two transmitters located at Karstadt and Universitaet, respectively. For the transmitter located at Karstadt we used 1420 field measurements and for the transmitter located at Universitaet we used 2140 field measurements.

Figs. 12 and 13 show the predictions for ray tracing and the radiance model. The ray tracing algorithm models energy transfers by shooting rays from the location of the antenna. When a ray reaches a surface, a reflected ray is generated. When a ray hits an edge, diffraction rays are generated according to the UTD solution [35]. In general, the results of both methods show a good agreement between measures and predictions for both transmitters. The correlation coefficient and the mean error show that the predictions follow the major trends. This is confirmed by the statistics shown in Table I. The radiance model shows a more accurate solution for most points. The difference in predictions is accounted for two main reasons. First, the radiance model includes scattering (i.e., diffuse reflection component) in the form of a specular-reflection exponent. In some cases, scattering is produced due to the size of the facets or due to its reflectance properties. The large number of surface interactions required for modeling diffuse scattering and diffractions limits the ray tracing solution of wave guiding effects resulting in errors in deep shadow regions. The differences in the results can also be explained by the fact that, whilst ray tracing shoots energy in the major directions from point to point, the radiance model gathers and integrates energy from visible surfaces at different resolutions. As such, the solution is found not as pure energy transfer, but as the equilibrium of energy. This produces a more accurate model of facet interactions. Previous work on light modeling have shown that methods based on radiance transfers provide an accurate treatment of inter-object reflections.

The radiance model can produce accurate predictions for many points. However, the results show some errors. Differ-

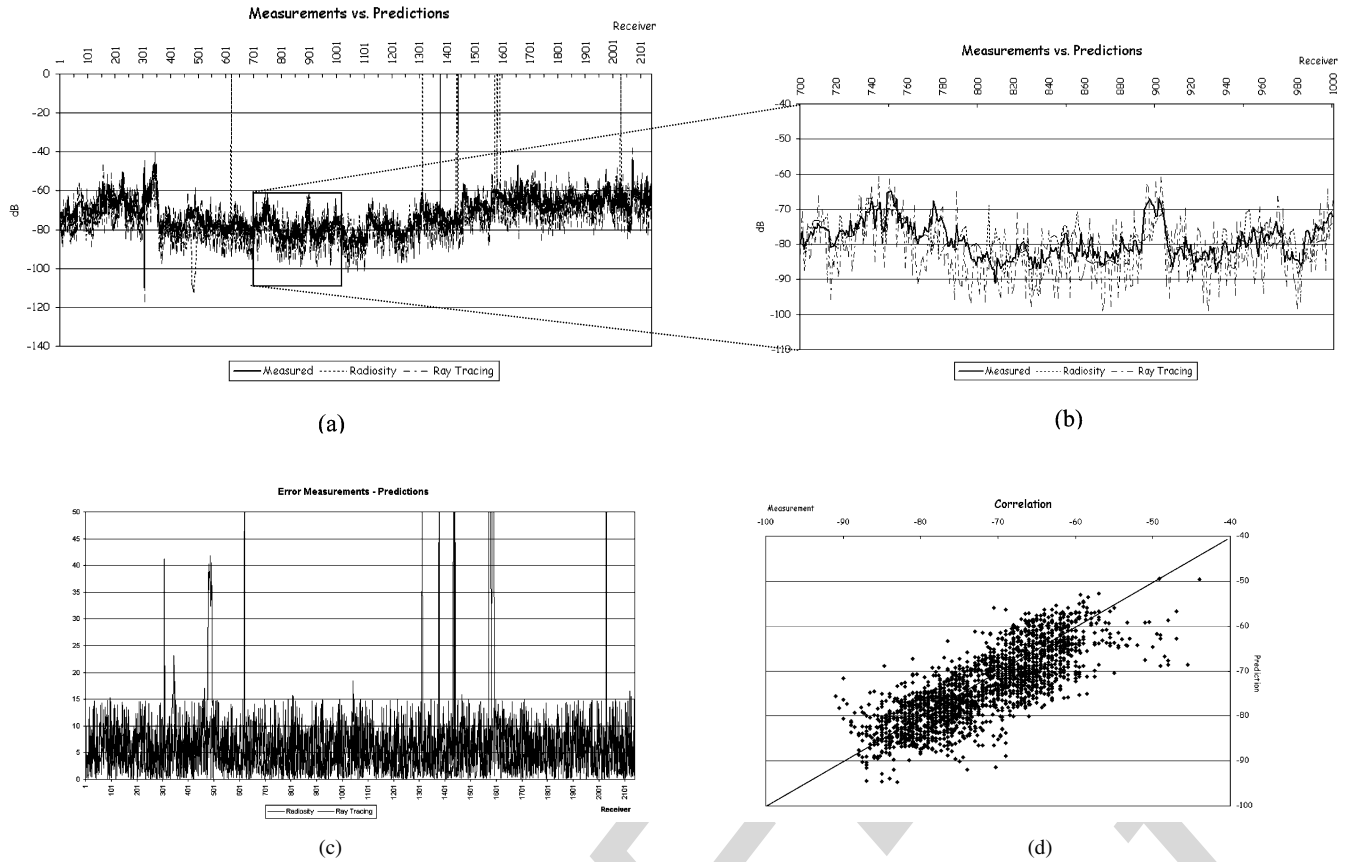

Fig. 13. Comparison of predicted values versus measurements for the transmitter located at Universitaet. (a) Measurements versus Predictions. (b) Detail of Measurements versus Predictions. (c) Error between measurements and predictions. (d) Correlation between Measurements and Predictions.

TABLE I
STATISTICS OBTAINED BY COMPARING MEASUREMENTS VS. PREDICTIONS FOR THE TWO TRANSMITTERS LOCATED IN STUTTGART

Statistics	Karstadt		Universitaet	
	Radiosity	Ray Tracing	Radiosity	Ray Tracing
Mean Error (dB)	0.22	3.94	1.77	3.42
Standard Deviation Error	6.64	8.01	6.61	8.07
Correlation	0.771	0.729	0.695	0.541

ences between measurements and radiance predictions are due to three main factors. First, there are some predictions with infinite path loss shown as zero values in the graphs. This is mainly due to lack of information in the database. For these points the contribution comes from a building that it is not present in the database, as such reflection is not obtained by the model and the point prediction does not have a value. This is a typical case for the receivers near the limit of the database (i.e., the dark regions in the border of Fig. 11). A second source of error is the limited number of reflections in the model. In some cases the signal power can be significant after several reflections. However, computations limit the possible number of interactions. The results presented in this paper were obtained by considering sixth order reflections. A better strategy could adaptively control the number of reflections and diffractions to minimize computation maximizing energy transfers. Finally, a third source of error comes from the fact that we consider that all buildings have the same reflective properties. In general, the absorption and aperture of reflections are not homogeneous for all the buildings. Thus, these parameters should be set for different areas of the database. However, this can be computationally complex.

VII. CONCLUSION

We have implemented a model of path-loss prediction based on global facet-to-facet radiance transfers. The model is based on radiosity techniques and it considers the visibility geometry of the power transfer between surfaces. The main differences between our model and radiosity techniques are: 1) our model considers diffraction; 2) it models specular and diffuse scattering; and 3) it considers fading effects. Since the diffuse component is neglected, then the equilibrium equation can be solved for just specific directions using iterative methods. Our implementation is based on the hierarchical radiosity algorithm. This efficiently handles facet subdivisions necessary to obtain an accurate prediction. Results show a good agreement with data

measurements capable of providing accurate propagation predictions. The main drawback is that it requires a fair estimate of the reflective properties of facets.

ACKNOWLEDGMENT

The authors would like to thank Alcatel Mobile Communications, France for providing the measurement data and Dr. S. Saunders for proof reading the paper.

REFERENCES

[1] C. López Giovaneli, "An analysis of simplified solutions for multiple knife-edge diffraction," *IEEE Trans. Antennas Propagat.*, vol. AP-32, pp. 297–301, Mar. 1984.
[2] J. Walfish and H. L. Bertoni, "A theoretical model of UHF propagation in urban environments," *IEEE Trans. Antennas Propagat.*, vol. AP-38, pp. 1788–1796, Dec. 1988.
[3] IEEE Transactions on Vehicular Technology, vol. 37, Special Issue on Mobile Radio Propagation, no. 1, 1988.
[4] G. Liang and H. L. Bertoni, "A new approach to 3-D ray tracing for propagation prediction in cities," *IEEE Trans. Antennas Propagat.*, vol. 46, pp. 853–863, 1998.
[5] J. W. Ikegami, T. Takeuchi, and S. Yoshida, "Theoretical prediction of map field strength for urban mobile radio," *IEEE Trans. Antennas Propagat.*, vol. 39, pp. 299–302, 1991.
[6] J. W. McKown and R. L. Hamilton, "Ray tracing as a design tool for radio networks," *IEEE Network Mag.*, vol. 5, no. 6, pp. 27–30, 1991.
[7] K. R. Schaubach, N. J. Davis, and T. S. Rappaport, "A ray tracing method for predicting path loss and delay spread in microcellular environments," in *Proc. IEEE Vehicular Technology Conf.*, 1992, pp. 932–935.
[8] R. A. Valenzuela, "A ray tracing approach to predicting indoor wireless transmission," *Proc. IEEE Vehicular Technology*, pp. 214–218, 1993.
[9] D. J. Cichon and W. Wiesbeck, "Ray optical wave propagation modeling in urban micro cells," in *Proc. PIMRC'94*, 1994, pp. 407–410.
[10] V. Erceg, A. J. Rustako, and R. S. Roman, "Diffraction around corners and its effects on the microcell coverage area in urban and suburban environments at 900 MHz, 2 GHz, and 7 GHz," *IEEE Trans Vehic. Technol.*, vol. 43, pp. 762–766, 1994.
[11] B. E. Gschwendtner, G. Wölfle, and F. M. Landsforfer, "Ray tracing versus ray launching in 3-D microcell modeling," in *Proc. European Personal and Mobile Communications Conf., EPMCC'95*, 1995, pp. 74–79.
[12] J. P. Rossi, J. C. Bic, and A. J. Levy, "A ray launching method for radio—mobile propagation in urban area," in *Proc. IEEE Antennas Propagation Symp.*, 1991, pp. 1540–1543.
[13] S. Y. Tan and H. S. Tan, "Propagation model for microcellular communications applied to path loss measurements in Ottawa city streets," *IEEE Trans. Veh. Technol.*, vol. 44, no. 2, pp. 313–317, 1995.
[14] C. M. Goral, K. E. Torrance, D. P. Greenberg, and B. Battaile, "Modeling the interaction of light between diffuse surfaces," *Computer Graphics*, vol. 18, pp. 213–222, 1984.
[15] F. X. Sillion and C. Puech, *Radiosity and Global Illumination*. San Francisco, CA: Morgan Kaufmann , 1994.
[16] C. Kloch and J. B. Andersen, "Radiosity—an approach to determine the effect of rough surface scattering in mobile scenarios," in *Proc. IEEE Antennas and Propagation Society Int. Symp.*, Montreal, Canada, 1997, pp. 890–893.
[17] K.-F. Tsang, W.-S. Chan, D. Jing, K. Kang, S.-Y. Yuen, and W.-X. Zhang, "Radiosity method: a new propagation model for microcellular communication," in *Proc IEEE Antennas and Propagation Soc. Int. Symp.*, vol. 4, 1998, pp. 2228–2231.
[18] C. Kloch, G. Liang, J. B. Andersen, G. F. Pedersen, and H. L. Bertoni, "Comparison of measured and predicted time dispersion and direction of arrival for multipath in a small cell environment," *IEEE Trans. Antennas Propagat.*, vol. 49, pp. 1254–1263, Sept. 2001.
[19] L. Neumann and A. Neumann, "Radiosity and hybrid methods," *ACM Trans. Graphics*, vol. 14, no. 3, pp. 233–265, 1995.
[20] D. Parsons, *The Mobile Radio propagation Channel*. New York: Wiley, 1992.
[21] P. Hanrahan, D. Salzman, and L. Aupperle, "A rapid hierarchical radiosity algorithm," *Computer Graphics*, vol. 25, no. 4, pp. 197–206, 1991.
[22] N. Dadoun, D. Kirkpatrick, and J. Walsh, "The Geometry of Beam Tracing," in *Proc. ACM Symp. Computational Geometry*, 1985, pp. 55–61.
[23] S. Coorg and S. Teller, "Temporally coherent conservative visibility," in *Proc. 12th Symp. Computational Geometry, ACM*, 1996, pp. 78–87.
[24] R. McCluney, *Introduction to Radiometry and Photometry*. London, U.K.: Artech House, 1994.
[25] J. T. Kajiya, "The rendering equation," *Computer Graphics*, vol. 20, no. 4, pp. 143–150, 1986.
[26] T. Nishita and E. Nakamai, "Continuous tone representation of three-dimensional objects taking account of shadows and interreflection," *Computer Graphics*, vol. 18, pp. 23–30, 1984.
[27] R. Siegel and J. R. Howell, *Thermal Radiation Heat Transfer*. New York: McGraw Hill, 1981.
[28] M. F. Cohen and J. R. Wallace, *Radiosity and Realistic Image Synthesis*. New York: Academic, 1993.
[29] D. S. Immel, M. F. Cohen, and D. P. Greenberg, "A radiosity method for nondiffuse environments," *Computer Graphics*, vol. 20, no. 4, pp. 133–142, 1986.
[30] L. Neumann and A. Neumann, "Photosimulation: interreflection with arbitrary reflectance models and illumination," *Computer Graphics Forum*, vol. 8, no. 1, pp. 21–34, 1984.
[31] A. Fournier, "Separating reflection functions for linear radiosity," in *Proc. Eurographics Workshop Rendering*, 1995, pp. 296–305.
[32] R. Lewis, "Making shaders more physically plausible," *Eurographics'94*, vol. 13, no. 3, pp. 1–13, 1994.
[33] M. Z. Shao, O. S. Peng, and Y. D. Liang, "A new radiosity approach by perocedural refinements for realistic image synthesis," *Computer Graphics*, vol. 22, no. 4, pp. 93–101, 1988.
[34] L. Neumann and A. Neumann, "Efficient radiosity methods for nonseparable reflectance models," in *Proc. Eurographics Rendering Workshop on Photosimulation Realism and Physics in Computer Graphics*, 1990, pp. 83–102.
[35] D. A. McNamara, C. W. I. Pistorius, and J. A. G. Malherbe, *Introduction to the Uniform Geometrical Theory of Diffraction*. Norwood, MA: Artech House, 1990.

Eugenia Montiel received the Ph.D. degree from the University of Southampton, Southampton, U.K., in 1997. Her dissertation research was on recursive functions.

During her Postdoctoral at iMAGIS at INRIA Rhône-Alpes, France, she worked on the implementation of radiosity techniques for radio wave simulation. She was a Research Assistant at the Centre for Communications Systems Research (CCSR), University of Surrey, Guilford, U.K., developing deterministic models for digital broadcasting. Currently, she is a Senior Software Developer at Cellular Design Services Ltd., Horsham, West Sussex, U.K. Her work focuses on the development of propagation and optimization models.

Alberto S. Aguado received the Ph.D. degree from the University of Southampton, Southampton, U.K., in 1997. His research work focused on image processing and shape extraction techniques.

In 1997, he obtained a Marie Curie fellowship European grant to work as a Research Fellow at INRIA, Rhône-Alpes, France. He worked as a Lecturer in the Centre of Vision Speech and Signal Processing (CVSSP) at the University of Surrey, Guilford, U.K. Currently, he is with the Character Core Group in EA, U.K. His research interests include shape modeling, shape extraction, fractals and topology, motion estimation, and stereo matching.

François X. Sillion is a Senior Researcher with INRIA and head of the ARTIS project in Grenoble, France. His research interests include the simulation of radiative transfer in complex scenes, with applications to realistic image synthesis, plant growth simulation and remote sensing; the simplification of complex models for realtime visualization; the capture and modeling of styles for expressive computer rendering.

Dr. Sillion serves on the editorial board of the *ACM Transactions on Graphics and Computer Graphics Forum*, and is a Member of the IEEE Computer Society, ACM Siggraph, and Eurographics.